AZIMUTHAL DISTRIBUTIONS IN INTERMEDIATE ENERGY HEAVY-ION COLLISIONS

By

William Kenneth Wilson

A DISSERTATION

Submitted to
Michigan State University
in partial fulfillment of the requirements
for the Degree of

DOCTOR OF PHILOSOPHY

Department of Physics and Astronomy

1991

ABSTRACT

AZIMUTHAL DISTRIBUTIONS IN INTERMEDIATE ENERGY HEAVY-ION COLLISIONS

By

William Kenneth Wilson

The azimuthal distributions of light particles (Z=1,2) with respect to the entrance channel reaction plane are investigated with a view towards characterizing the modes of collective motion in intermediate energy heavy-ion collisions. A new technique for reaction plane determination from the distribution of light particles produced in a collision is developed and applied to Ar+V data. The data were acquired using the MSU 4π Array, a new 215 element large solid angle detector system. At a beam energy of 35 MeV/nucleon, light charged particles are found to exhibit an enhanced emission in the reaction plane which increases with the mass of the detected particle. As the beam energy is increased to 100 MeV/nucleon, the anisotropy nearly vanishes, providing clues to the dynamics of these reactions in a transitional energy regime.

The observed anisotropy contains signatures of two distinct modes of collective motion: attractive mean field deflection, and rotation of the fused system. A microscopic calculation based on mean-field mediated interactions plus nucleon-nucleon collisions reproduces both forms of collective motion and their associated azimuthal distributions. The calculation also suggests that the anisotropy due to mean-field deflection is established during the initial stages of the collision.

The nature of the nuclear mean-field is further explored using data taken by the

4π Array for peripheral 50 MeV/nucleon C induced reactions on C and Au targets. Although projectile fragments in grazing collisions are positively deflected by the coulomb force, a specific set of protons are found to be simultaneously attractively deflected by the mean-field towards the opposite side of the reaction plane. This direct observation of attractive mean field deflection supports aspects of the interpretation of the Ar+V data.

Lastly, the experimental results are summarized and the potential for extracting more information about the dynamics of heavy-ion collisions using azimuthal distributions is assessed. The key areas of promising future experimental research in this subject are delineated along with the outstanding problems to be solved.

Dedicated with love to Mary.

ACKNOWLEDGEMENTS

A heartfelt "thank you" goes to my research advisor, Gary Westfall. Without Gary's blend of patience, encouragement, and enthusiasm, it would not have been possible for me to reach the end of this project. More importantly, Gary's irrepressible sense of humor made the process fun. I benefited from his guidance and teaching during each step of the experiments and analysis. Whoop.

This work was also shaped by important contributions from Craig Ogilvie and Roy Lacey. It was a joy discussing my analysis with them and leaving a trail of "Hindenburgs" on the blackboards all over the lab. Special credit must be given to Craig, who originally developed the reaction plane determination technique presented in chap. 3.

Several people deserve thanks for their generosity in donating their time to various aspects of this project. Wolfgang Bauer performed the theoretical calculations presented in chap. 6, and guided me in their interpretation. Skip Vandermolen, Pawel Danielewicz, and Dennis Swan answered innumerable questions, and seemed to enjoy pondering each new problem I brought to them. Len Morris turned my rough sketches into functioning detector mounts for the Forward Array. Chadin Djalali, David Kroftcheck, and Thierry Reposeur provided moral support.

It has been a pleasure working with the other graduate students at the Cyclotron Lab, past and present. Jim Clayton, Dan Fox, Dan Cebra, Jeff Karn, Steve Howden, Mats Cronqvist, Brian Young, and Tong Li have helped, encouraged, and shared their knowledge with me, making this project easier than it would have been otherwise.

I owe a great debt to my parents and my wife for putting up with the agony and ecstasy of a physics graduate student. My parents displayed unshakable confidence in me, and supported all of my decisions that led me over a circuitous route to this

final result. My wife Mary Samuel generously gave of herself to help me through the darkest times, and so I dedicate this thesis to her. Since she read and commented on this thesis, she is literally on every page.

Advice from Epictetus (ca. 50-138 A.D.) "*When a man is proud because he can understand and explain the writings of Chrysippus, say to yourself, 'If Chrysippus had not written obscurely, this man would have nothing to be proud of.'* "

Contents

List of Tables

List of Figures

Chapter 1

Introduction

In this thesis we will investigate the properties of heavy-ion collisions at beam energies ranging from near the Fermi energy ($\approx$ 37 MeV/nucleon) to 100 MeV/nucleon. The motivation for studying these collisions is two fold. Ultimately, we hope to contribute to the characterization of the bulk properties of nuclear matter. No results which constrain the properties of nuclear matter will be presented in this initial analysis, but techniques which may do so in the future will be developed. The more immediate aim of this work is simply to characterize the dynamics of the events. These reactions are quite complex because they involve a finite number of particles which have access to a nearly innumerable number of final states. Therefore, detailed descriptions of these collisions should provide motivation and some of the tools for improving our ability to calculate the dynamics of complex finite systems in general.

This beam energy region is particularly interesting because it is expected to be transitional. At beam energies just above the Coulomb barrier, reactions are dominated by the attractive component of the nuclear mean field. **Central collisions** (head on) result in compound nucleus formation, while **peripheral collisions** give rise to an attractive deflection of the projectile or its capture to form an orbiting system. On the other hand, at relativistic beam energies, the overlap region of the projectile and target becomes highly compressed, and the hard core repulsive compo-

nent of the nuclear mean field comes into play. The beam energy range studied in this thesis spans the region in which the dominant interaction is expected to change from attractive to repulsive. We will refer to this as the **intermediate energy** range.

Since progress was made in the understanding of relativistic collisions by confronting theory with the observed modes of collective motion, we will maintain this approach in our examination of intermediate energy collisions. Collective motion occurs with respect to the plane initially containing the beam axis and target, called the **reaction plane**. We will focus particularly on azimuthal distributions with respect to the reaction plane, which we find to be useful indicators of the presence of collective motion.

In order to determine the reaction plane from the final distribution of particles, it is generally necessary to detect as many of the outgoing particles as possible. To this end, a large acceptance detection system called the **MSU 4π Array** was constructed. The data taken with the MSU 4π and presented in this thesis represent some of the first explorations of collective motion in intermediate energy collisions.

1.1 Organization

The organization of this thesis is as follows. In the introduction we will begin by introducing some of the concepts used in describing bulk nuclear matter. Since our work began as an extension of the approaches employed to characterize relativistic collisions, we will also review what was learned about collective motion in relativistic collisions. Finally we will outline some of the differences between the collision dynamics at relativistic beam energies and those expected at intermediate energies.

In the second chapter we will describe the experimental apparatus and early stages of the analysis. Chapter three presents the technique we have developed to determine

the reaction plane for central and medium impact parameters. The next chapter presents our data in the form of azimuthal distributions of particles with respect to the reaction plane. The observed anisotropies are interpreted in terms of simple modes of collective motion. The data will be compared to a microscopic calculation in the fifth chapter, and we will draw conclusions about the nature of observed collective motion. In the sixth chapter we will shift the focus to analysis of peripheral events, in which we will be able to observe the attractive nature of the nuclear mean-field directly. Finally, in the seventh chapter, we will summarize what has been learned and suggest possible directions for future development. Subjects on the periphery of the main thread of the thesis have been placed in appendices to streamline the presentation.

1.2 The Bulk Properties of Nuclear Matter

Outside of neutron stars and perhaps the early universe, infinite nuclear matter exists only as a theoretical construct used to test our understanding of the nuclear force. For example, if we can deduce the equation of state of bulk nuclear matter from nucleus-nucleus collisions, this would provide some guidance to theorists attempting to write down the strong force Hamiltonian in a baryon-rich environment.

Two properties of infinite nuclear matter are apparent from the examination of nuclei in there ground state.[Wong90] From letting the atomic mass number A go towards infinity in the Weizacker semi-empirical mass formula, and ignoring the Coulomb force, we find the the binding energy (E_b) per nucleon is

$$E_b \approx 16 MeV. \tag{1.1}$$

We also know that nuclear matter saturates at a density

$$\rho_o \approx 0.17 \,\text{nucleons fm}^{-3} \tag{1.2}$$

from the study of the charge distribution in heavy nuclei. Thus we can demand that the nuclear **equation of state (EOS)**, which describes how nuclear matter responds to changes in density, reproduce these values. One commonly used form of this expression is[Bert88]

$$U(\rho) = A\frac{\rho}{\rho_o} + B\left(\frac{\rho}{\rho_o}\right)^{\sigma}, \tag{1.3}$$

where $U(\rho)$ is the density dependent potential field and σ is greater than one. In eq. 1.3 the constant A is attractive (negative) and the constant B is repulsive (positive). The EOS is usually taken as the nuclear compressional potential energy (E_{cp}) as a function of density given by

$$U(\rho) = \frac{\partial}{\partial\rho}(\rho E_{cp}) \tag{1.4}$$

The unknown factors A, B, and σ can be fixed in terms of binding energy, saturation density, and a new parameter K, the **nuclear compressibility**. The compressibility is defined as $\frac{9}{\rho}$ times the bulk modulus k, which is the logarithmic derivative of the pressure with respect to the density. A derivation of these equations can be found in [Bert88]. The compressibility K is a measure of how difficult it is to push the system away from its equilibrium density, and is thus important in certain astrophysics applications. For example, it determines the density of neutron stars and the propagation of shock waves created in supernova explosions. In Figure 1.1 we show the nuclear compressional energy (the sum of the potential energy and the Fermi energy) as a function of density for two different values of the compressibility.[Moli85a]

Larger values for K would mean that it takes more energy to compress nuclear matter, a situation referred to as a **stiff** equation of state, while smaller values indicate a **soft** EOS. The compressibility can only be inferred from observing the properties of nuclear matter away from the equilibrium density. Placing constraints on K has

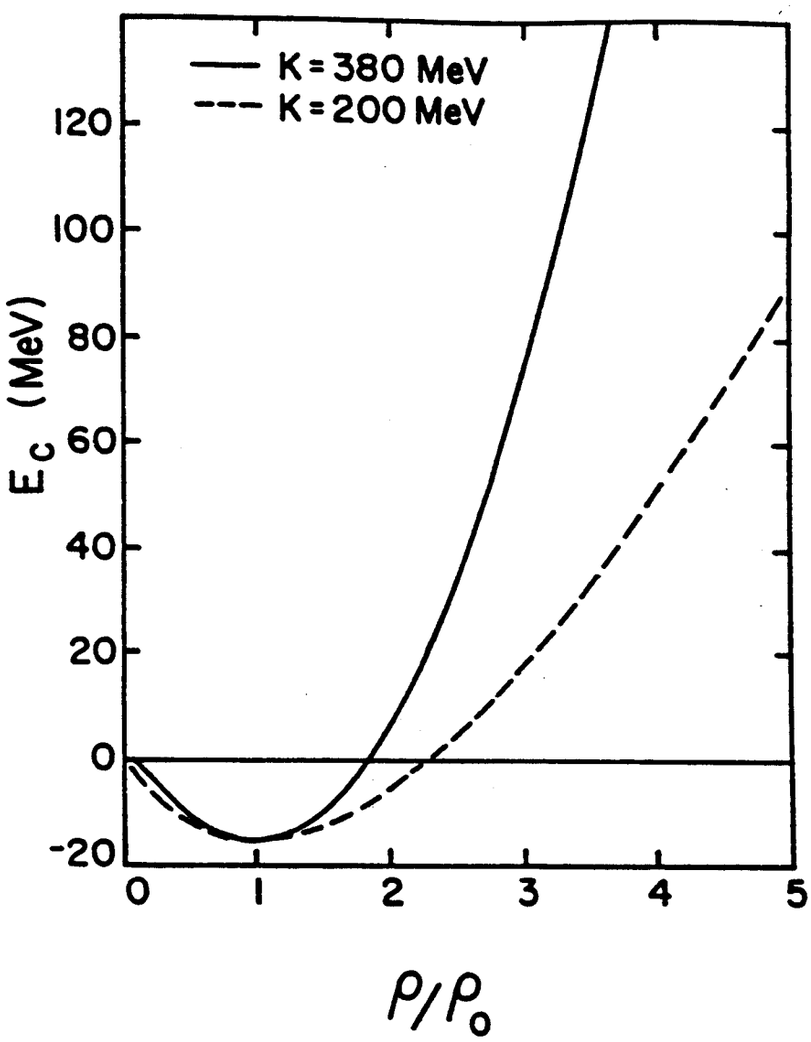

Figure 1.1: The equation of state for two different values of the compressibility of nuclear matter.[Moli85a]

been one of the major goals of heavy-ion physics. In Figure 1.2 we show the results of several different techniques used to measure K, including the flow angle measurements of relativistic heavy-ion collisions which will be described in detail in this introduction. The best constraints placed on the equation of state so far have come from the study of frequency of vibrating nuclei (giant monopole resonance).[Shar89] (The new data on vibrating nuclei result from the systematic study of a larger number of nuclei than the original data.) The extremely low K values found to be necessary in simulations of supernovae are thought to represent a failing of current supernova theory. We can conclude from the graph that the compressibility is $\approx$ 300 MeV with large error bars. In the next section, we review how the study of relativistic heavy-ion collisions has been used to constrain the equation of state.

1.3 Review of Results from Relativistic Heavy-Ion Collisions

Beams of **relativistic heavy-ions** (Z> 4, E_{beam} >100 MeV/nucleon) became available at Lawrence Berkeley Laboratory (LBL) in 1974. Early experiments, which detected only one particle per event, showed that particles were produced by three distinct sources. A **participant-spectator** geometry was successfully applied describe the observed energy spectra.[West76] In this picture, the parts of the projectile and target that do not overlap during the collision (spectators) are less strongly disturbed. The projectile remnant forms a **projectile-like source** which continues on with nearly the same velocity as the original projectile, and similarly the target remnant forms a **target-like source**. The overlapping participant region forms a hot **fireball** whose velocity and excitation energy can be deduced from the assumption of a completely inelastic collision and clean cut geometry, as shown in Figure 1.3. We will use this terminology to describe sources of light particles in chap. 6.

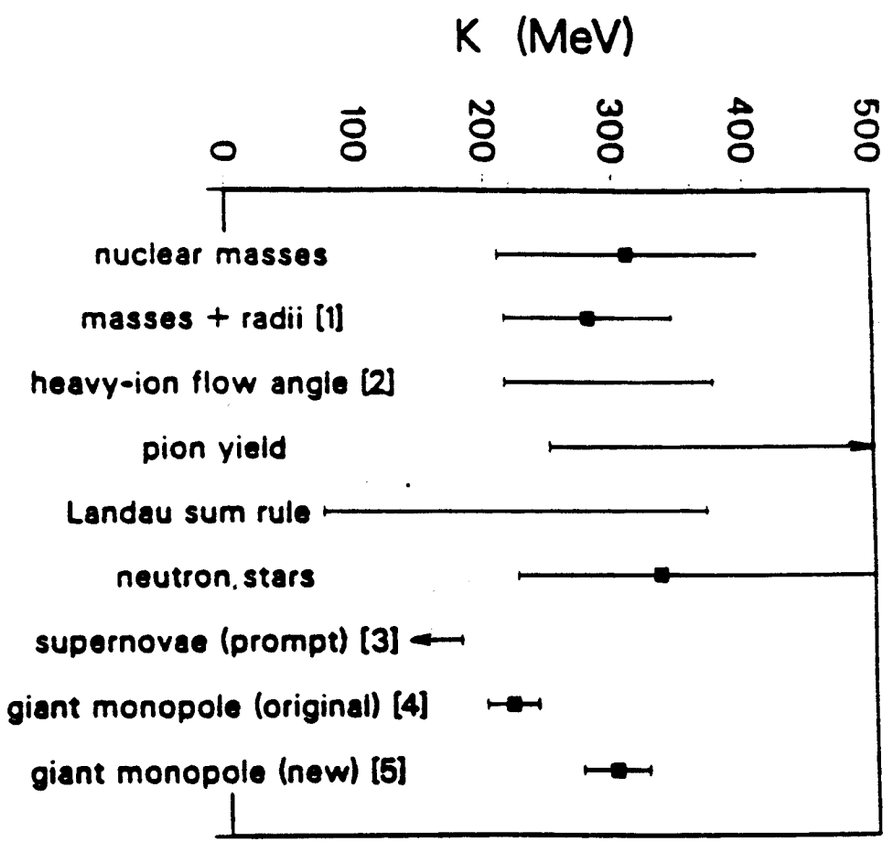

Figure 1.2: Summary of measurements of K.[Glen88]

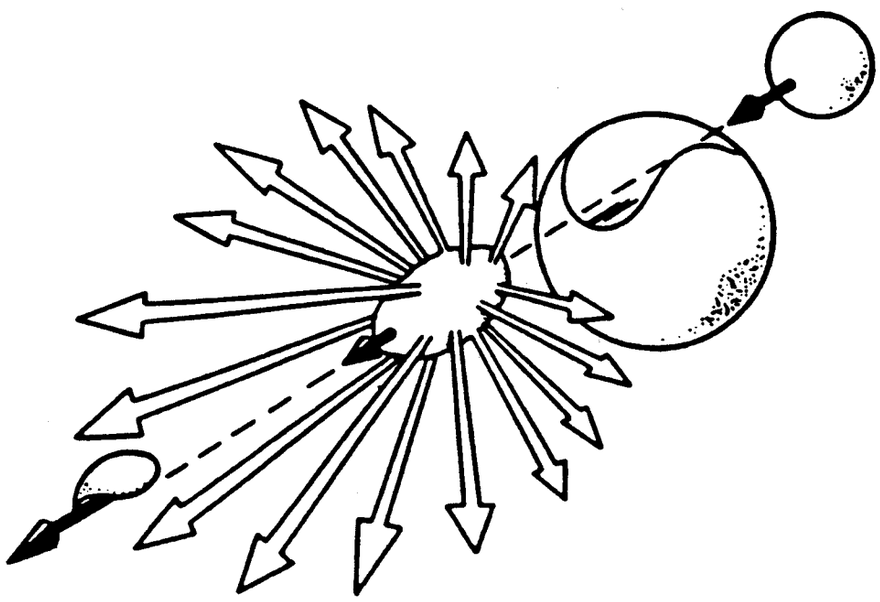

Figure 1.3: The participant-spectator geometry used in the Nuclear Fireball Model.[West76]

Early experiments did not provide enough information about the collisions to distinguish definitively between competing models of reaction mechanisms because they were mainly single particle experiments. It was the observation of collective motion using detectors capable of observing many particles in each event that played the central role in driving forward the theory of relativistic reactions.

Two of the early competing models were the **Hydrodynamic Model**[Stöc82, Buch84] and the **Intranuclear Cascade.**[Yari79, Cugn83] In figure 1.4 we show the results of fluid-dynamical and cascade calculations for the system 400 MeV/nucleon Nb+Nb. Note that there is a considerable **side-splash** of nucleons in the final frame of the hydrodynamical calculation, while the cascade produces a more nearly isotropic distribution.

The hydrodynamical model assumes that the mean free path of nucleons in nuclear matter is very short, leading quickly to **local equilibrium**, and allowing the nuclear matter to be treated **macroscopically** in terms of variables like pressure and temperature. The short mean free path causes compressional energy to be built up very efficiently, leading to the side-splash or **collective flow**[Stöc80] observed in the figure. One drawback of the theory is that real heavy-ion collisions involve a finite number of particles, not a smooth continuum, making it difficult to compare the calculations to actual observations of nuclei, especially in collisions of lighter ions.[Stöc86]

Intranuclear cascade calculations avoid this problem since they track the progression of each nucleon through time. For this reason they are referred to as **microscopic** calculations, and need not assume local equilibrium. The nucleons interact with each other only through collisions, whose cross sections are taken from free nucleon nucleon scattering. This causes the nuclei to be more transparent to each other than in the hydrodynamical model, and the lack of compressional energy shows up in the weaker collective flow in the figure. Since there is no **mean field** created by the

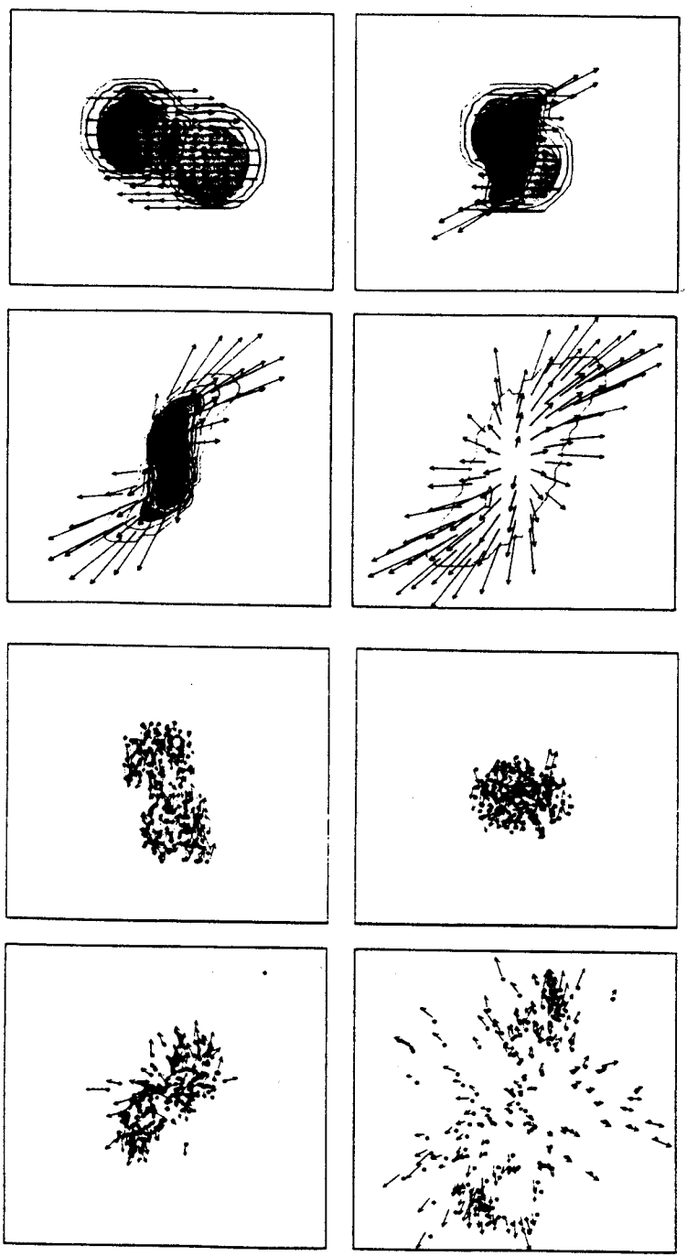

Figure 1.4: Fluid dynamical (top panels) and cascade (bottom panels) calculation of a 400 MeV/nucleon Nb+Nb collision. The impact parameter is 3 fm and $\approx$ 10 fm/c in time separates the snapshots. [Grei85] The view is looking down on the reaction plane. The beam axis is left to right in the upper panels and top to bottom in the lower panels.

nucleons, there is no potential well and thus the Fermi momentum causes nuclei to be unstable. Therefore an undisturbed nucleus will evaporate nucleons over time. This flaw can be overcome by several artificial initialization procedures, but it reflects the incompleteness of the cascade picture.[Stöc86] Due to the lack of a proper quantum mechanical initialization, quantum effects such as the Pauli exclusion principle cannot be included during the calculation of reactions.

Because the azimuthal angle (around the beam axis) of the reaction plane varies randomly from event to event, the effects of collective flow tend to average out for single particle observables. For example, both models could reproduce the energy spectra and angular distributions observed using one detected particle per event. To provide more sensitivity to collective effects, large acceptance detection systems were developed to measure as many charged particles as possible emerging from a single event, allowing determination of the event's shape in momentum space. From the shape of the event, experimentalists could determine the reaction plane and then rotate each event to a common orientation. Quantities could then be measured relative to the reaction plane, eliminating azimuthal averaging. We will take up the details of reaction plane determination in the third chapter.

The two primary experimental facilities which were used to study collective flow were the LBL Streamer Chamber and the Plastic Ball. A computer reconstruction of a Streamer Chamber image is shown in Figure 1.5. Because the violence of relativistic collisions can lead to the total disintegration of the projectile and target in central collisions, the charged particle multiplicity can exceed 100. The Plastic Ball[Gutb89a] consisted of more than 1000 charged particle detectors, arranged into an modified icosahedron plus a forward array.

In 1985 Danielewicz and Odyniec[Dani85] developed a method of displaying the experimental data that made it possible to quantify reliably the side-splash in the

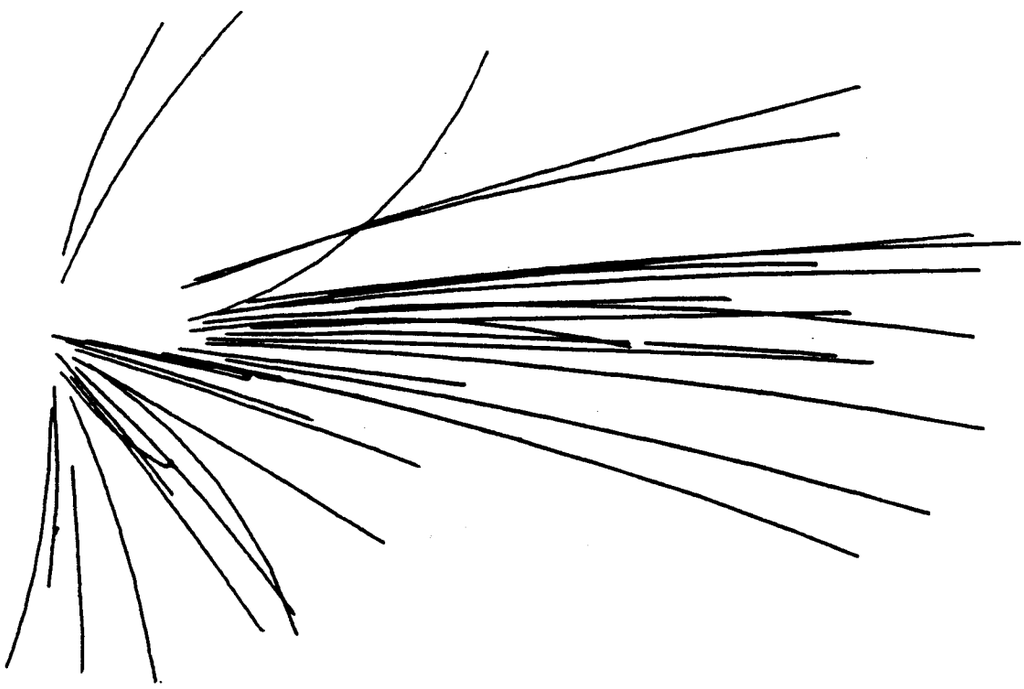

Figure 1.5: Computer reconstruction of the tracks seen on a Streamer Chamber photographic plate. The projectile (not visible) enters from the left travelling horizontally. This was a central collision of a relatively light system, Ar+KCl at 1.8 GeV/nucleon. A magnetic field perpendicular to the page produces the curvature observed in the tracks. (Positive ions curve clockwise, negative pions curve counterclockwise.)[Bibb85]

participant zone. This **transverse momentum analysis** is illustrated in Figure 1.6 for 400 MeV nucleon Nb+Nb central collisions. The side-splash is revealed by plotting the average transverse momentum projected into the reaction plane as a function of rapidity. The **rapidity** variable (y) is a Galilean invariant function of the velocity parallel to the beam axis $\beta_{||}$,

$$y = \frac{1}{2} \ln \left(\frac{1 + \beta_{||}}{1 - \beta_{||}} \right). \tag{1.5}$$

If the velocity is small compared to the speed of light, then the rapidity reduces to $\beta_{||}$. The slope of the transverse momentum as a function of rapidity is called the **flow**, and can be compared to theoretical models once the uncertainty in the reaction plane determination is taken into account.

Danielewicz et al. found that the hydrodynamical model over-predicted the flow, while the intranuclear cascade under-predicted it. Clearly, the assumption of local equilibrium and a very short mean free path in the hydrodynamical model was an approximation. A new model was developed that retained the microscopic approach of the intranuclear cascade, but added an additional interaction mediated by the nuclear mean field.[Bert88] The addition of the mean field interaction requires a specific value of the compressibility (K) in the equation of state, so the effects of a soft versus a stiff EOS on the collective flow could be evaluated. The treatment of collisions in the cascade model was also carried over to the new calculation. The new approach goes by different names, each group of theorists coining their own terminology, such as **Boltzmann-Uehling-Uhlenbeck (BUU)**,[Uehl33, Bert84] **Vlasov-Uehling-Uhlenbeck (VUU)**,[Krus85] **Boltzmann-Nordheim equation**,[Nord28] or **Landau-Vlasov equation**.[Greg87] We will compare our observations to BUU theory in the fifth chapter.

The comparisons between the initial BUU simulations and the flow observed in

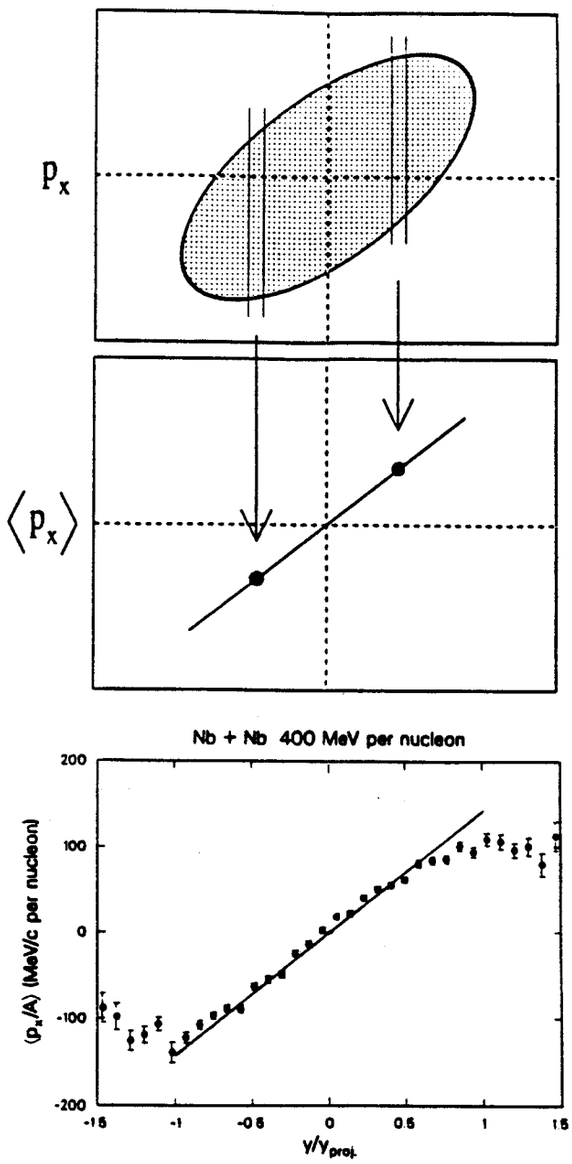

Figure 1.6: Explanation of transverse momentum analysis used for measuring the collective flow of the participants. The top panel is a schematic picture of the momentum distribution, the bottom panel is the average transverse momentum in the reaction plane as a function of rapidity for actual Plastic Ball data.[Gutb89a]

heavy-ion reactions led to a surprisingly stiff equation of state, $K \approx 380$ MeV.[Moli85a, Dani88] This was much higher than the value being used in supernova calculations, for example. Later, it was discovered that inclusion of the expected momentum dependence of the nuclear interaction into eq. 1.3 could reproduce the observed flow using a lower compressibility of ≈ 200 MeV.[Gale87] This trade off between K and momentum dependent interactions produces the large uncertainty bars in Figure 1.2. Thus, we can conclude that observations of relativistic heavy-ion collisions have the potential to constrain the equation of state, dependent on improvements of microscopic models and a better understanding of nucleon-nucleon collisions in nuclear matter.

In 1989,[Gutb89b] a new component of the collective motion was discovered, the so-called **squeeze-out** in which the compression of the participant zone forces particles out of the reaction plane at mid-rapidity.[Gutb90] Squeeze-out, illustrated in Figure 1.7, was also predicted by hydrodynamical models.[Stöc86]

The Plastic Ball data on collective motion are summarized by the plots in figs. 1.8 and 1.9. We see that both the flow and the squeeze-out peak at a beam energy around 300 to 400 MeV/nucleon. (The flow in Figure 1.8 has been rendered beam energy scale invariant in a manner suggested by hydrodynamical considerations.[Bona87]) The magnitude of both effects drops rapidly as the beam energy is decreased towards 100 MeV/nucleon. This trend can be understood in terms of the competition between the attractive and repulsive components of the nuclear mean field visible in Figure 1.1. At the lower beam energies, the compression is too small to access the density region dominated by hard core repulsion for very long, and longer range attractive part of the mean field becomes important. In fact, BUU calculations predict that the flow should actually change directions for lower beam energies.

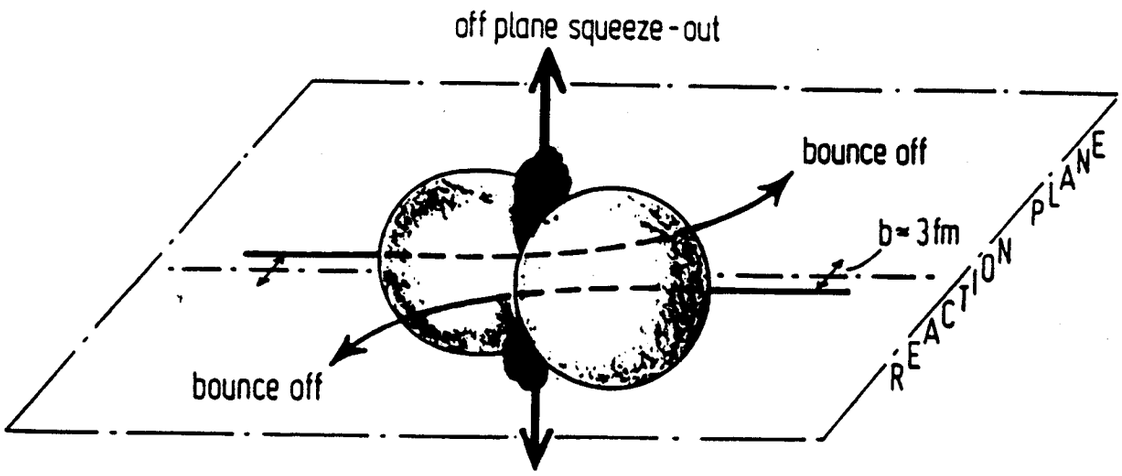

Figure 1.7: Illustration of the squeeze-out effect predicted by fluid dynamics.[Stöc86]

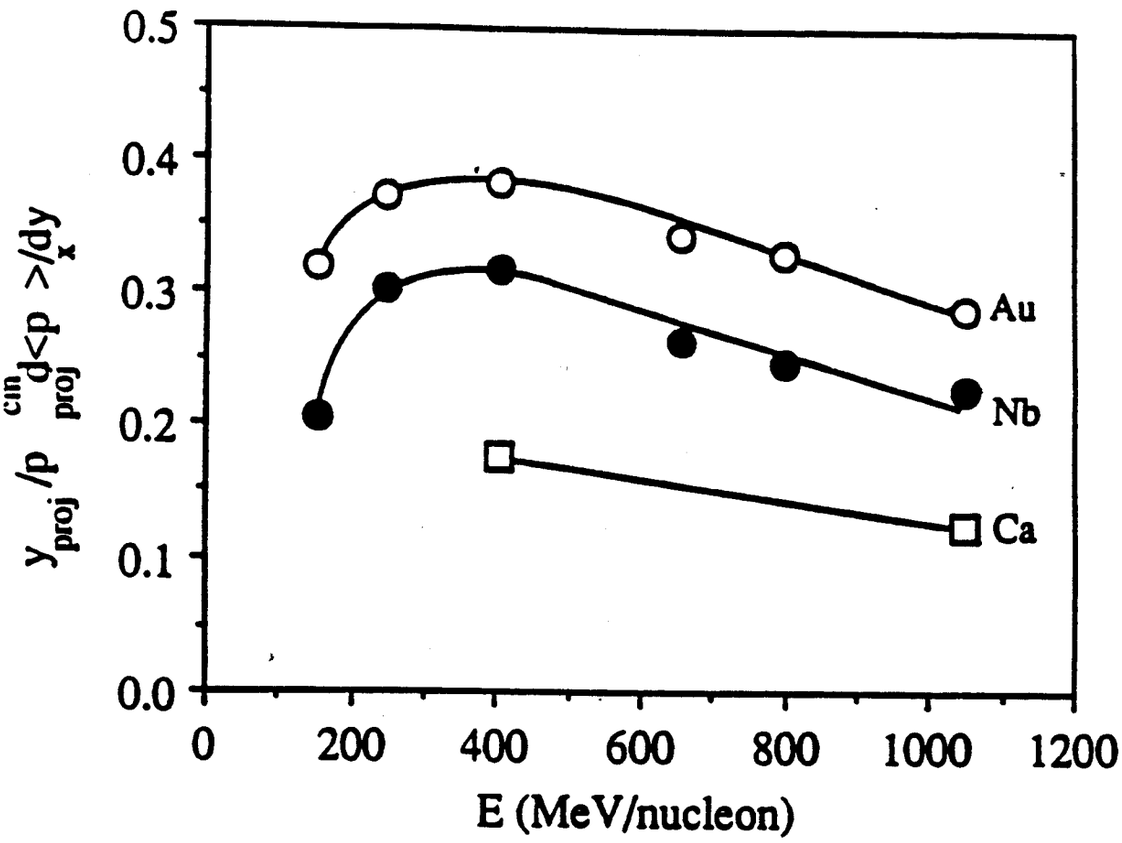

Figure 1.8: Flow as a function of beam energy in heavy-ion collisions in data taken with the Plastic Ball.[Schm91] The scaled flow (F) is proportional to the slope of the transverse momentum projected into the reaction plane as a function of rapidity, and calculated at mid-rapidity

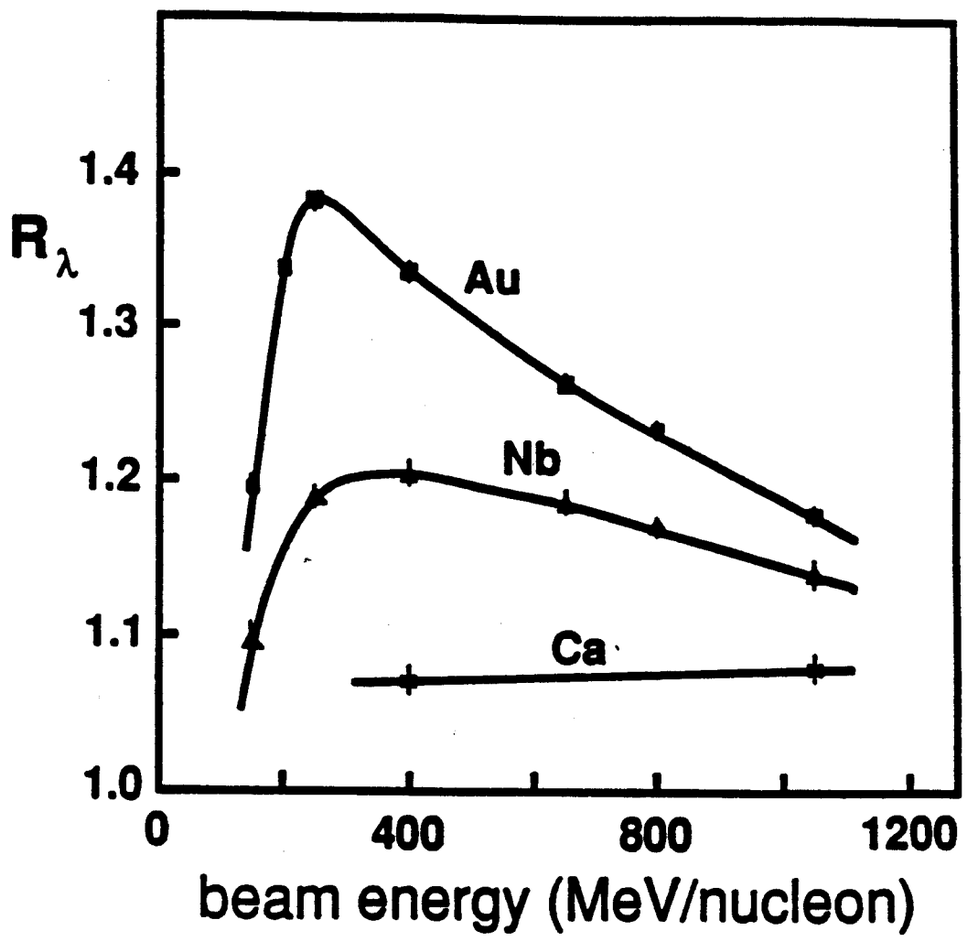

Figure 1.9: Squeeze-out as a function of beam energy in heavy-ion collisions in data taken with the Plastic Ball.[Schm91] The squeeze-out ratio (R) is the ratio of the out-of-plane to in-plane axis of an ellipsoid used to parameterize the observed momentum distribution.

1.4 Extension to Lower Beam Energies

In Figure 1.10 we show schematically the difference between repulsive flow, in which the particles are pushed away from the high compression region, and attractive flow where the particles are deflected negatively. These sketches should not be taken as a detailed description of the momentum distributions produced in these collisions, but as a simplification of the collective motion in the mid-rapidity region. BUU calculations, shown in Figure 1.11 performed by Molitoris et al.[Moli85b] predicted "inverted" flow at beam energies around 50 MeV/nucleon for the Nb+Nb system. Later BUU calculations[Bert87] have also produced attractive flow in systems of mass 40 projectile on mass 40 to 197 targets at beam energies $\leq$ 100 MeV/nucleon.

The attractive nature of the nuclear force in collisions with beam energies on the order of 10 MeV/nucleon has been established experimentally. We will review here two examples, Wilczyński orbiting and residue gamma ray polarization.

In 1973, Wilczyński plotted the cross section for production of K fragments in 9.7 MeV/nucleon Ar+Th collisions as a function of both center of mass (c.m.) energy and angle.[Wilc73] This novel mode of presenting the data, shown in Figure 1.12, revealed the relationship between two components in the observed energy spectra.[Artu73] Wilczyński's interpretation is shown schematically in Figure 1.13. He held that the ions observed near the beam energy had been repulsively scattered by the Coulomb force in peripheral collisions, while the ions in the lower energy peak resulted from collisions with smaller impact parameters in which the attractive mean field caused the projectile to orbit partially the heavier target. Note that although the sign of the scattering angle of a single particle is undetermined, the overall pattern shows the effects of both positive and negative scattering.

Collisions of the latter sort are said to be **deep inelastic**, with the velocity of the

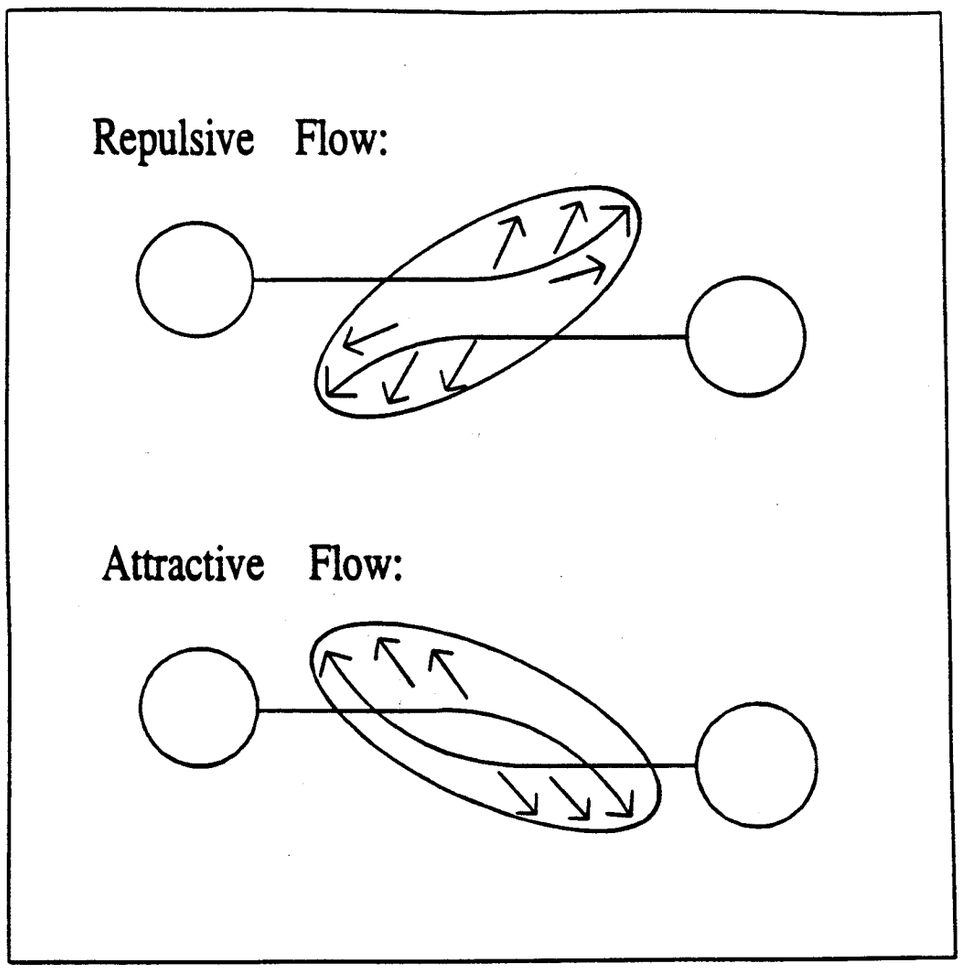

Figure 1.10: The difference between the concepts of attractive and repulsive flow.

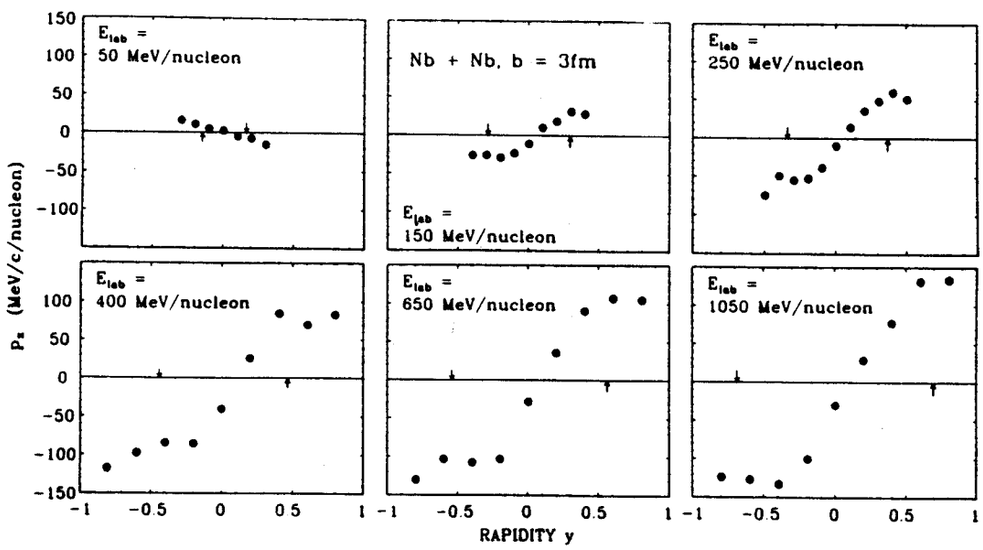

Figure 1.11: BUU predictions of average transverse momentum in the reaction plane as a function of rapidity is shown for the Nb+Nb for several beam energies. Note that the flow is inverted in the lowest beam energy calculation.[Moli85b]

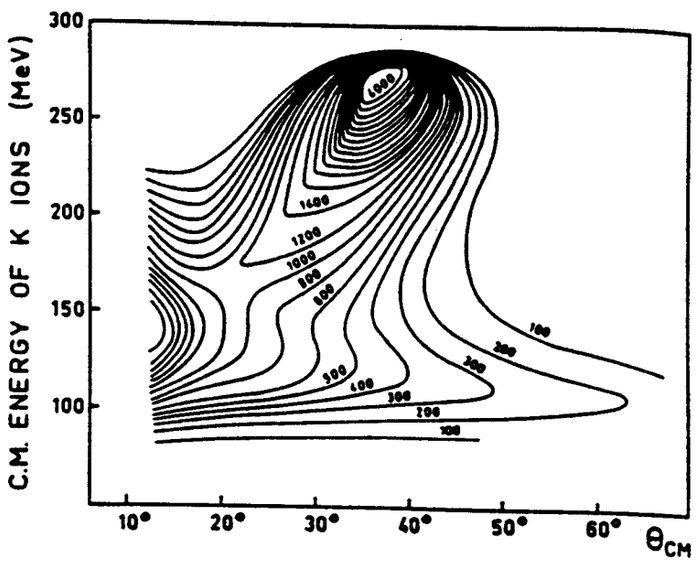

Figure 1.12: Contour map of the K cross section produced in 9.7 MeV/nucleon Ar+Th collisions. ,This method of presenting the data is called a **Wilczyński plot.**[Wilc73]

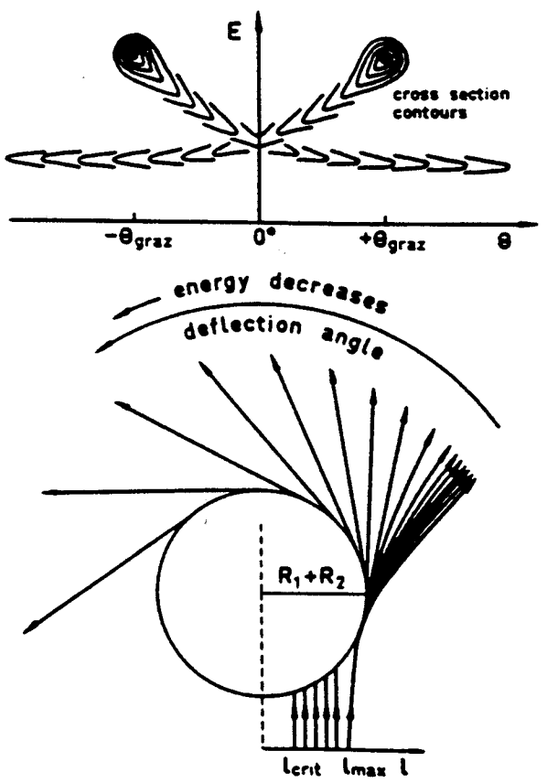

Figure 1.13: Scattering processes which create the ridges on a Wilczyński plot.[Wilc73]

projectile being strongly **damped**. The most peripheral collisions are referred to as **quasi-elastic** since the projectile fragment appears with almost all of the projectile's original momentum per nucleon. If the beam energy is above the Coulomb barrier, central collisions result in **fusion** forming a compound nucleus that can have a large amount of rotational collective motion which is dissipated by neutron and gamma ray emission.[Step65]

The circular polarization of the deexcitation gamma rays can be exploited to measure the direction of the mean field deflection directly when detected in coincidence with charged particles. Observation of collisions of O and N projectiles ranging from 8 to 35 MeV/nucleon with Nb and Sm targets indicate that high energy light particles are attractively deflected by the nuclear mean field.[Trau84, Tsan86] Further direct evidence for the attractive nature of mean field deflection in these energy ranges will be presented in chap. 6 using data taken using the MSU 4π Array.[Wils91]

The goal of this thesis is to investigate the transitional regime in which attractive mean field deflection gives way, as the beam energy is increased, to compressional phenomena such as side-splash and squeeze-out. We will do this by classifying the modes of collective motion that we observe at 35 MeV/nucleon, and investigating their evolution as the beam energy is increased to 100 MeV/nucleon.

1.5 Earlier Observations of Collective Motion in Intermediate Energy Collisions

Beyond the mean-field deflection described earlier, the only other evidence of possible collective motion in this transitional beam energy regime has come from the two particle correlation measurements of Tsang et al. and Fox et al. Both experimental groups found that one light particle tends to be found preferentially in the

same plane as that defined by the beam axis and an additional light particle detected from the same event.[Tsan84a, Chit86, Fox88] In addition, Tsang and coworkers found that light particles are preferentially emitted in the same plane with respect to the beam axis as fission fragments detected in heavy ion collisions with Au and U targets.[Tsan84b, Tsan90] In Figure 1.14 we show the azimuthal distribution of alpha particles with respect to the reaction plane obtained by Tsang et al. for collisions with a U target. Since fission fragments produced in heavy-ion collisions are thought to be focused in the reaction plane,[Vaz83] a simultaneous explanation of all the correlation results was made by invoking the existence of a rotating source spinning off particles preferentially in the reaction plane. The angular momentum of such a source would originate from at least partial fusion between the projectile and target, so the angular momentum vector would be perpendicular to the reaction plane.

In our presentation of the data in chap. 4, we will use the idealized concepts of attractive flow, as shown in Figure 1.10, and a rotating source, as invoked by Tsang et al.,[Tsan84a] to provide a starting point for interpreting the data. In chap. 5 a more rigorous comparison between the data and these models will be carried out.

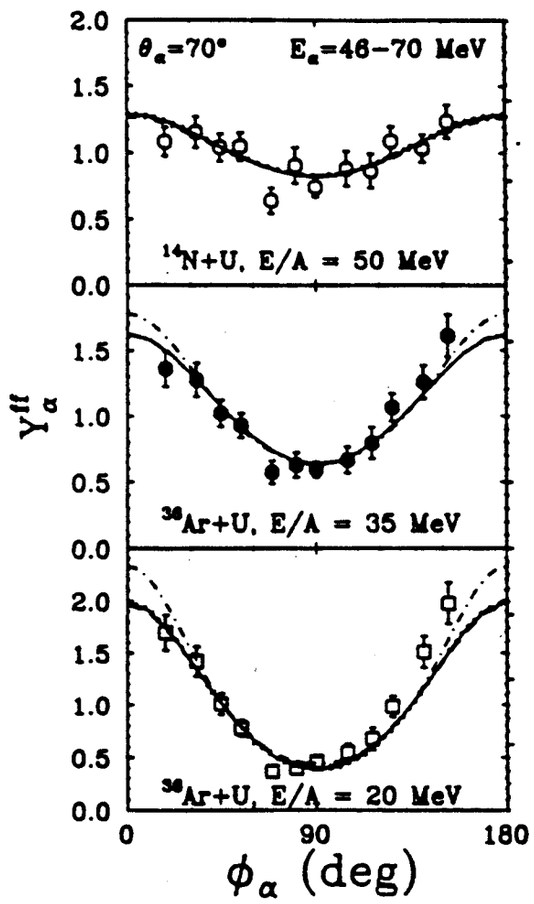

Figure 1.14: Azimuthal distribution of alpha particles around the reaction plane defined by fission fragments.[Tsan90]

Chapter 2

Description of the 4π Array Experiments

2.1 Beam and Target

The majority of the data presented in this thesis was taken using an ^{40}Ar projectile on a ^{51}V target. We chose this projectile because Ar was the heaviest ion that could be accelerated to beam energies up to 100 MeV/nucleon, increasing the probability that we could reach the regime where the dominant interaction becomes repulsive. V was the target closest to mass 40 available. It is desirable to have equal mass projectile and target because then it can be assumed that the projectile and target contribute equally to the participant (overlap) region, producing a source that moves with the center of mass velocity regardless of impact parameter.

A 35 MeV/nucleon Ar beam was produced by the MSU K500 superconducting cyclotron, and beams of 45, 55, 65, 75, 85, and 100 MeV/nucleon Ar were produced by the newer K1200 cyclotron. The target was a 3.34 mg/cm^2 V foil held in an aluminium frame. During the experiments, runs were also performed on an empty target frame to determine the amount of beam-frame interactions due to the possible presence around the beam spot of a low intensity halo. As a rule of thumb, the beam was focused until the target-in/target-out count rate ratio was greater than 10.

Ratios as high as 40 were not uncommon.

The beam current used varied from 50 to 100 electrical pA, depending on the amount available from the cyclotron and the count rate of the most forward large solid angle detectors. With beam bursts approximately every 50 ns, these currents corresponded to only 1 to 2 Ar ions in each burst, so the possibility of multiple events in a single beam burst was quite small and did not limit the allowed beam current. However, at detector count rates for single hits greater than $\approx$ 10000/second, the charge resolution was degraded due to pile up of signals, limiting the maximum beam current. Since this limit changes with the beam energy, the resolution of the detectors was monitored on line for any sign of reduced resolution and the beam current was adjusted accordingly.

For the chapter on peripheral events, a 50 MeV/nucleon ^{12}C beam from the K500 cyclotron was incident on ^{12}C and ^{197}Au targets. The asymmetric system C+Au was used in order to evaluate the role of momentum conservation recoil by comparison with the lighter C+C system. The C projectile allowed allowed detection of projectile fragments (particles close to the beam in charge that appear in the forward direction due to peripheral collisions) down to lower energies in relation to the beam energy than an Ar projectile.

2.2 Detector Geometry

The choice of the geometry for the 4π Array was primarily governed by two requirements. The geometry had to allow closest packing of detector modules to allow nearly full 4π angular coverage, and ideally the modules would be interchangeable. This second requirement simplifies construction and allows "speciality modules" to be easily swapped in for coincidence experiments. The geometrical shape that was chosen was

a 32 faced truncated icosahedron, similar to a soccer ball, shown in Figure 2.1.

Twenty of the faces are hexagonal, and twelve are pentagonal. Two of the pentagonal faces are reserved for beam entrance and exit; all of the remaining sites are filled by detector modules. Each module is further subdivided into the triangular wedges which make up the **Main Ball** telescopes, 5 wedges for the pentagonal and 6 for the hexagonal modules, 170 in all. We exploited a previously built set of 30 cylindrical and 15 rectangular telescopes to partially fill the beam exit pentagonal site as a **Forward Array.** They were arranged about the beam axis as is shown in figure 2.2.

The solid angles covered by the telescopes are shown in Table 2.1 for Main Ball detectors. The true solid angles are slightly smaller than those predicted by ideal geometry due dead spaces between the modules. The Forward Array telescopes subtend a solid angle of $\approx$ 3 msr each, bringing the total coverage of the Main Ball/Forward Array system to 84% of 4π.

Table 2.1: Solid Angles of Main Ball Telescopes

Module Type	Geometric (msr)	True (msr)
Hex	75.2	66.0
Pent	59.0	49.9

2.3 Detector Design

The detectors that make up the 4π Array are all of the same basic design, **phoswich** scintillator telescopes. As shown in Figure 2.3, the telescope is made of a thin layer of "fast" plastic scintillator in front of a larger piece of "slow" plastic scintillator which is optically coupled to a photomultiplier tube.[Wilk52] When any charged particle

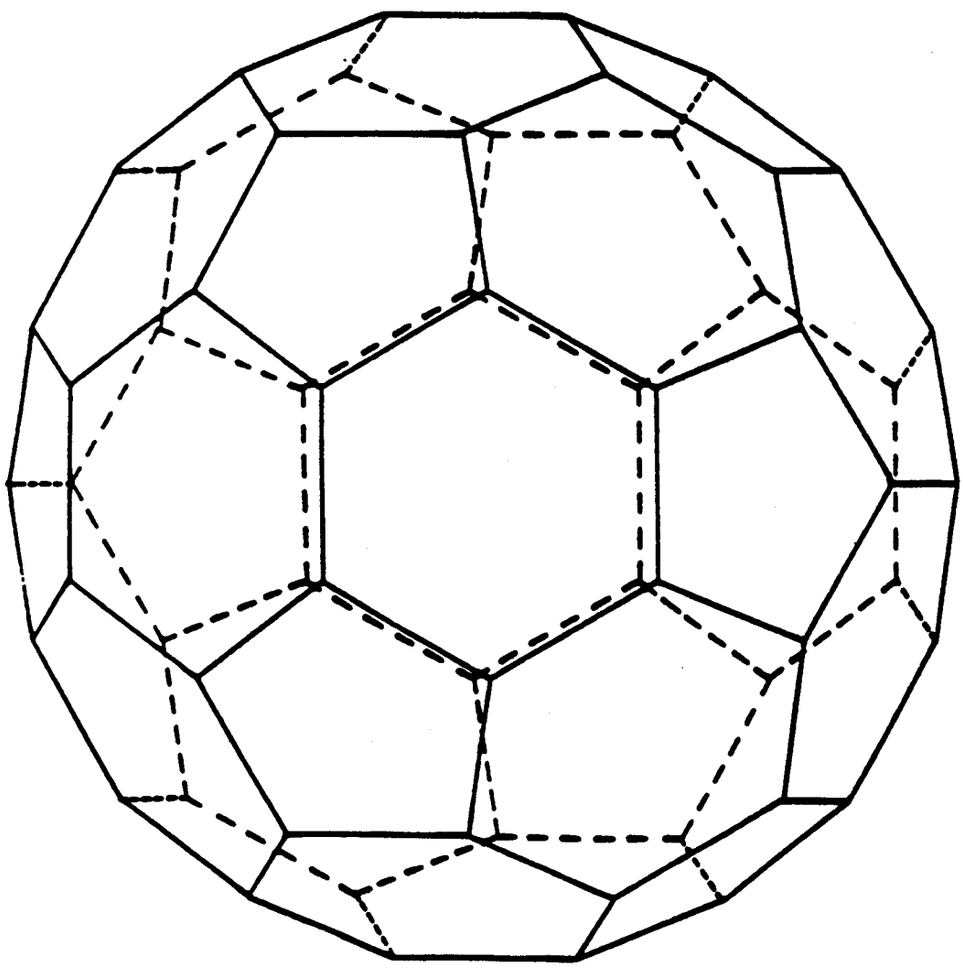

Figure 2.1: A truncated icosahedron, the basic geometry of the 4π Array

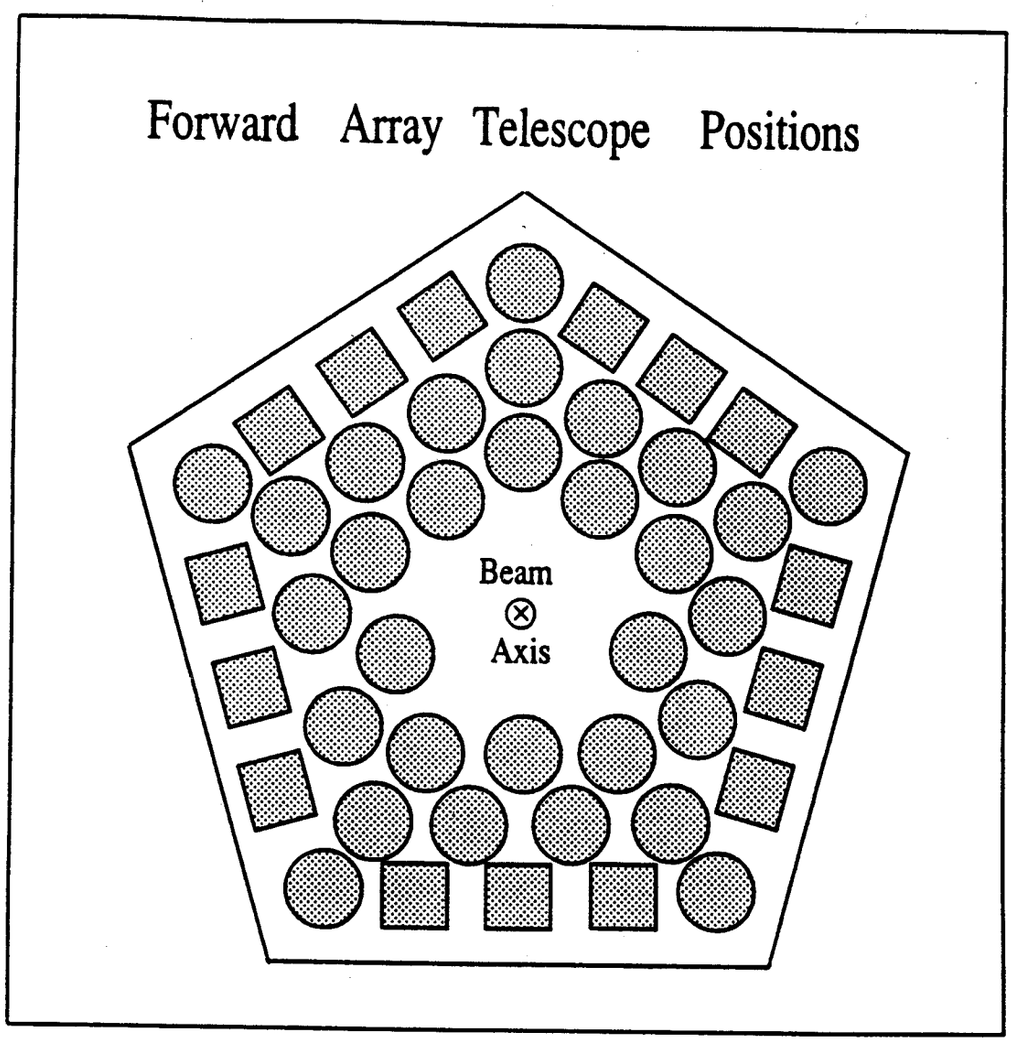

Figure 2.2: The positions of the front faces of the Forward Array telescopes. The beam axis goes into the page.

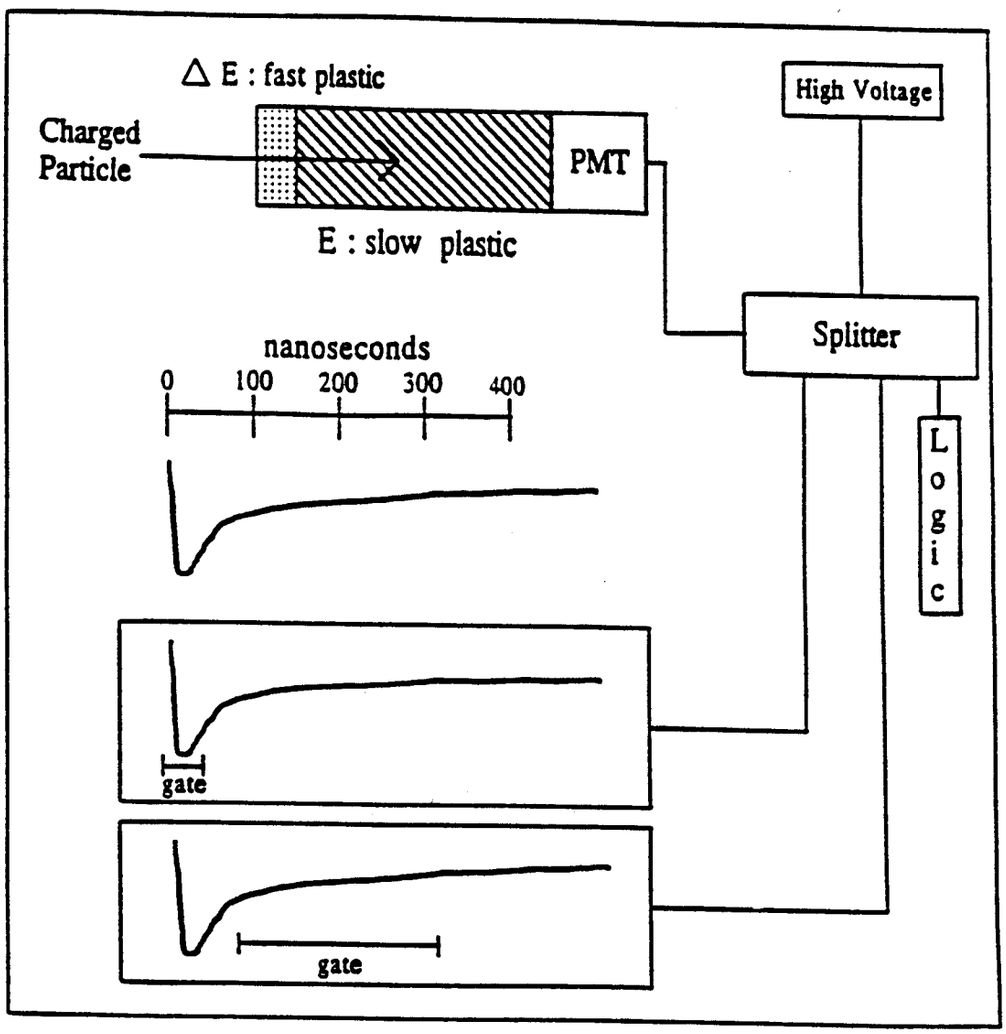

Figure 2.3: A phoswich (phosphor sandwich) detector. The positions of the gates used in the current integrating analog to digital converters (QDCs) are shown.

passes through the scintillator, its energy loss produces light, which is gathered by the photomultiplier tube and turned into a current pulse. The fast and slow plastic have shorter and longer decay times, shown in Table 2.2,[Bicr85] and thus their individual contributions to the current pulse can be separated. Figure 2.3 shows that the current from the photomultiplier is divided three ways: one stream is integrated over the time period during which the fast signal dominates, another is integrated to pick out the slow signal, while the third goes off to form the trigger stream, which will be discussed in Appendix A.

Table 2.2: Properties of the Fast and Slow Plastic Scintillators

BICRON plastic	rise time (ns)	fall time (ns)
BC-412 (fast)	1.0	3.3
BC-444 (slow)	19.5	179.7

The fast and slow components of the signal can be used together to identify charged particles which punch through the fast plastic using the **ΔE-E** technique. Since the energy loss is

$$-\frac{dE}{dx} \propto \frac{Z^2}{A} \tag{2.1}$$

at any given velocity, if the number of counts are plotted against the integrated fast (ΔE) and slow (E) signals, particles with different charges and masses will fall into different bands. A ΔE-E plot of 35 MeV/nucleon Ar+V data is shown in Figure 2.4 for a Forward Array telescope, and in Figure 2.5 for a Main Ball telescope. The characteristic features of a phoswich ΔE-E spectra are described schematically in Figure 2.6.

Particles with insufficient energy to punch through the fast plastic fall in the **punch-in line**. In this case, no energy is deposited in the slow plastic, but since the slow gate picks up a little of the decaying fast signal, the punch-in line has a finite

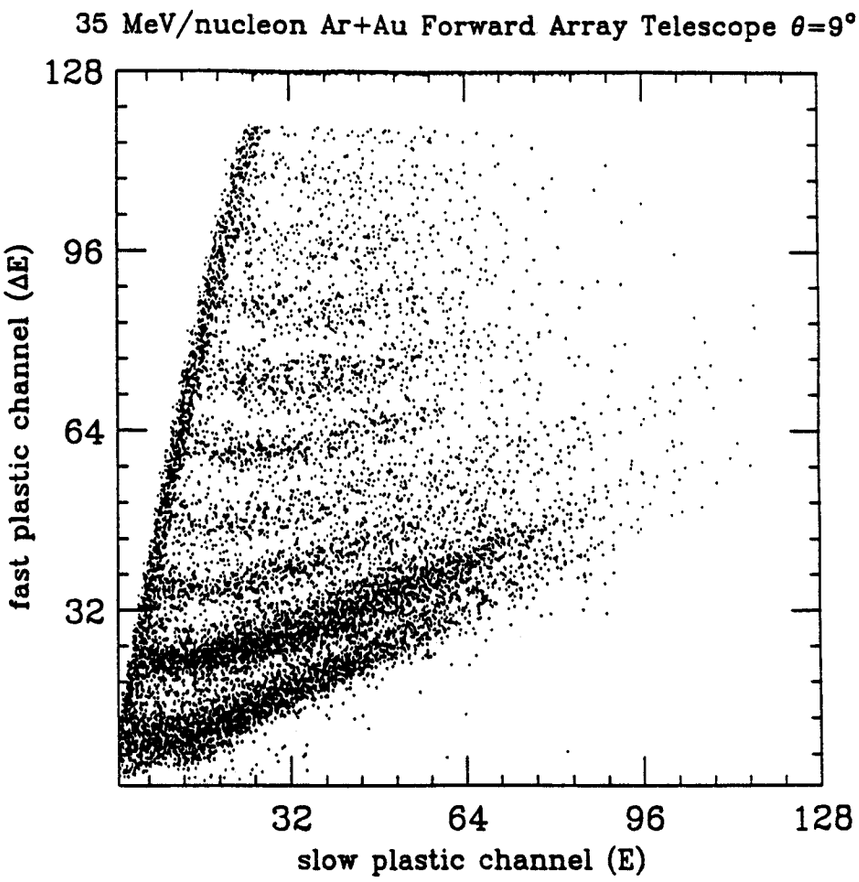

Figure 2.4: Counts as a function of the integrated fast (ΔE) and slow (E) signals for a Forward Array phoswich telescope.